Essential Supplementary Information (ESI)

Ultrastable and Highly Efficient Hydrogen Evolution by Heterogeneous NiO/Ni Catalysts in Industrial Electrolysis Conditions

Feng Chen[a], Wenfeng Peng[b], Junshuang Zhou[a]*, Xuezheng Ma[a], Yan Wang[a], Ying Zhang[a],Faming Gao[a]*

[a]Hebei Key Laboratory of Applied Chemistry, School of Environmental and Chemical Engineering, Yanshan University, Qinhuangdao 066004, China.

[b]School of Energy Engineering, Huanghuai University, Zhumadian, 463000, Henan, China.

* Corresponding authors.

E-mail: jszhou@ysu.edu.cn (J. Zhou), fmgao@ysu.edu.cn (F, Gao).

Experiment Section

Chemicals and Materials:

Hydrochloric acid (HCl, 36-38%, MACRON), ethanol (C_2H_5OH, AR, MACRON), nickel (II) chloride ($NiCl_2$, 98%, Macklin), sodium acetate ($C_2H_3NaO_2 \cdot 3H_2O$, AR, Aladdin) sodium dodecyl sulfate (SDS, AR, Aladdin), sodium citrate tribasic dihydrate ($C_6H_5O_7Na_3$, AR, Aladdin), potassium hydroxide (KOH, 95%, Macklin), nafion 117 solution (5%, Sigma-Aldrich), iridium oxide power (IrO_2, 99%, Alfa Aesar), platinum carbon (Pt/C, 98%, Aladdin). Copper foam (CF, thickness=1mm) was purchased from Guangshengjia new material Co. Ltd. Further processing is required before use. The deionized water used in all experiments was purified by the Millipore system.

Preparation of NiO/Ni@Cu, $Ni(OH)_2$@Cu and Ni@Cu:

Firstly, a piece of Cu foam with a size of 0.8×0.8 cm^2 was cleaned in hydrochloric acid (3 M) and then cleaned in ethanol and deionized water for 10 min sequentially. The deposition solution was prepared with 0.246 g sodium acetate and 0.5 g $NiCl_2$ in 30 ml deionized water. NiO/Ni@Cu was fabricated by constant current deposited at 90 mA cm^{-2} for 10 min in a two-electrode system by using Cu foam, Pt net as cathode and anode. As a comparison, $Ni(OH)_2$@Cu and Ni@Cu were prepared in the same way, except that sodium acetate was replaced with 0.01 g SDS and 0.882 g sodium citrate tribasic dihydrate.

Preparation of Pt/C and RuO_2 catalysts on NF:

Pt/C powder (8 mg, 20 wt%), and carbon black (4 mg, Vulcan XC72) were dissolved in a solution containing 50 μL Nafion, and 950 μL water/ethanol (V: V=1:1), and the mixture was uniformly dispersed by ultrasound for 30 min. The paste was then evenly coated on both sides of the treated copper foam and dried in a vacuum drying oven at 60°C for 12 h to produce an electrode loaded with Pt/C catalyst (denoted Pt/C). The RuO_2 electrode (denoted RuO_2) was prepared by the same procedure with RuO_2 powder (8 mg, 20 wt%).

Materials Characterization:

The phase structure of the samples was characterized with a powder X-ray diffractometer (XRD) (Cu Kα) at a scanning speed of 5° min^{-1} in the range of 10-90°. The morphology of the samples was observed by field emission scanning electron microscopy (SEM, SUPRA 55) and transmission electron microscopy (TEM, JEOL, JEM-2010). The composition and distribution of the elements of the samples were analyzed by energy-dispersive X-ray spectroscopy (EDS) attached to the transmission electron microscopy. The chemical composition and surface electronic states of the samples were studied by X-ray photoelectron spectroscopy recorded on an ESCA-LAB MKII device with a monochromatic Al-K-α X-ray source. The Fourier transform infrared spectroscopy with the attenuated total reflection were examined using a Nicolet-20DXB Fourier transform infrared spectrometer (FTIR).

Electrochemical Measurements:

All samples were tested for their electrochemical performance in a three-electrode system by using Shanghai C&H CHI660E at room temperature. A standard three-electrode system included a reference electrode (Hg/HgO), counter electrode (graphite rod), and the prepared samples were used directly as the working electrode (0.8×0.8 cm^2), respectively. The HER test was performed in 1 M and 6 M KOH at room temperature, respectively, while the water splitting test in 6 M KOH at 80°C. The linear scanning voltammetry (LSV) curve was performed at a sweep rate of 5 mV s^{-1} and the overpotential at different current densities was tested. To reveal the intrinsic behavior of the catalysts, 95% iR correction was employed to eliminate the effect of Ohmic resistance (expect all stability tests). All measured potentials were calibrated to a reversible hydrogen electrode (RHE) according to the Nernst equation: $E_{RHE}=E_{Hg/HgO}+0.098+0.059\times pH$. Unless otherwise stated, the potential values were relative to the reversible hydrogen electrode (vs. RHE) in this work and the Tafel slope from the LSV curve by plotting the potential against the logarithm (current density). The double-layer capacitance (C_{dl}) of the samples was calculated by cyclic voltammetry (CV) measurements at different sweep rates, in accordance with the electrochemically active surface area (ECSA). The capacitive current was linearly related to the scan rate, corresponding to a slope twice as large as C_{dl}. The electrochemical impedance (EIS) was measured at open circuit potential in the frequency range of 0.01 Hz to 100 kHz. The long-term stability was measured by the chronopotentiometry measurements for both HER and water splitting at a current density of 100 mA cm^{-2}.

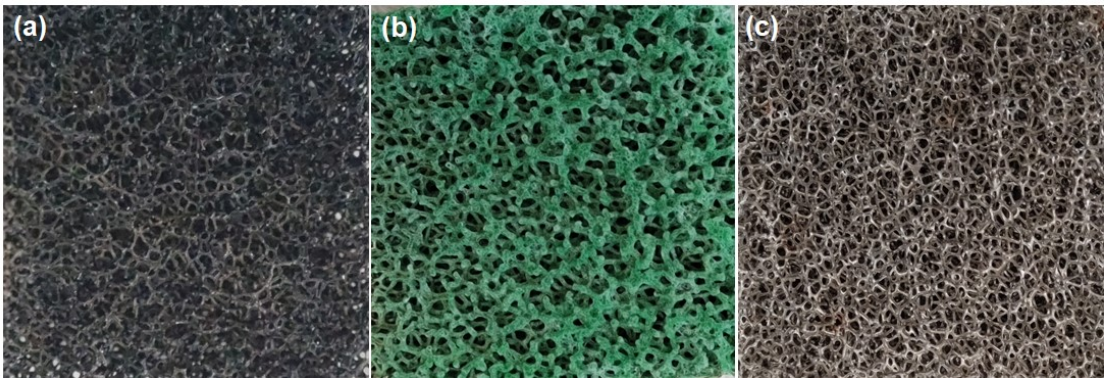

Figure S1. Optical diagram of (a) NiO/Ni@Cu, (b) $Ni(OH)_2$/Ni@Cu and (c) Ni@Cu.

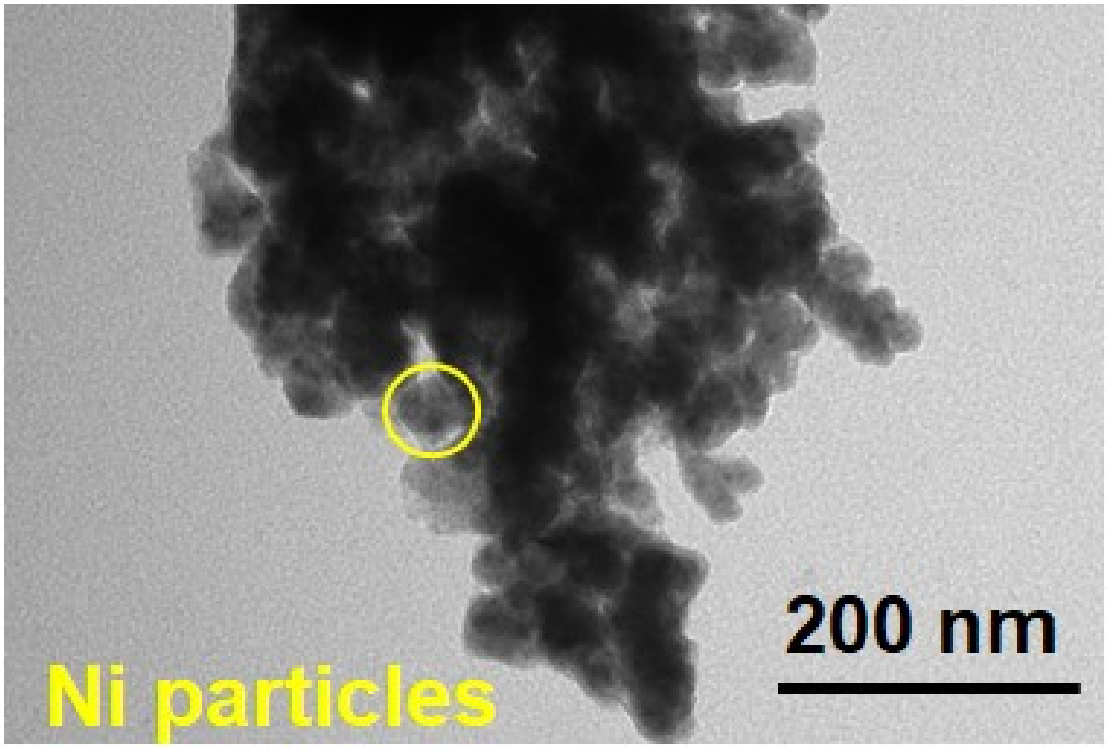

Figure S2. TEM images of NiO/Ni@Cu.

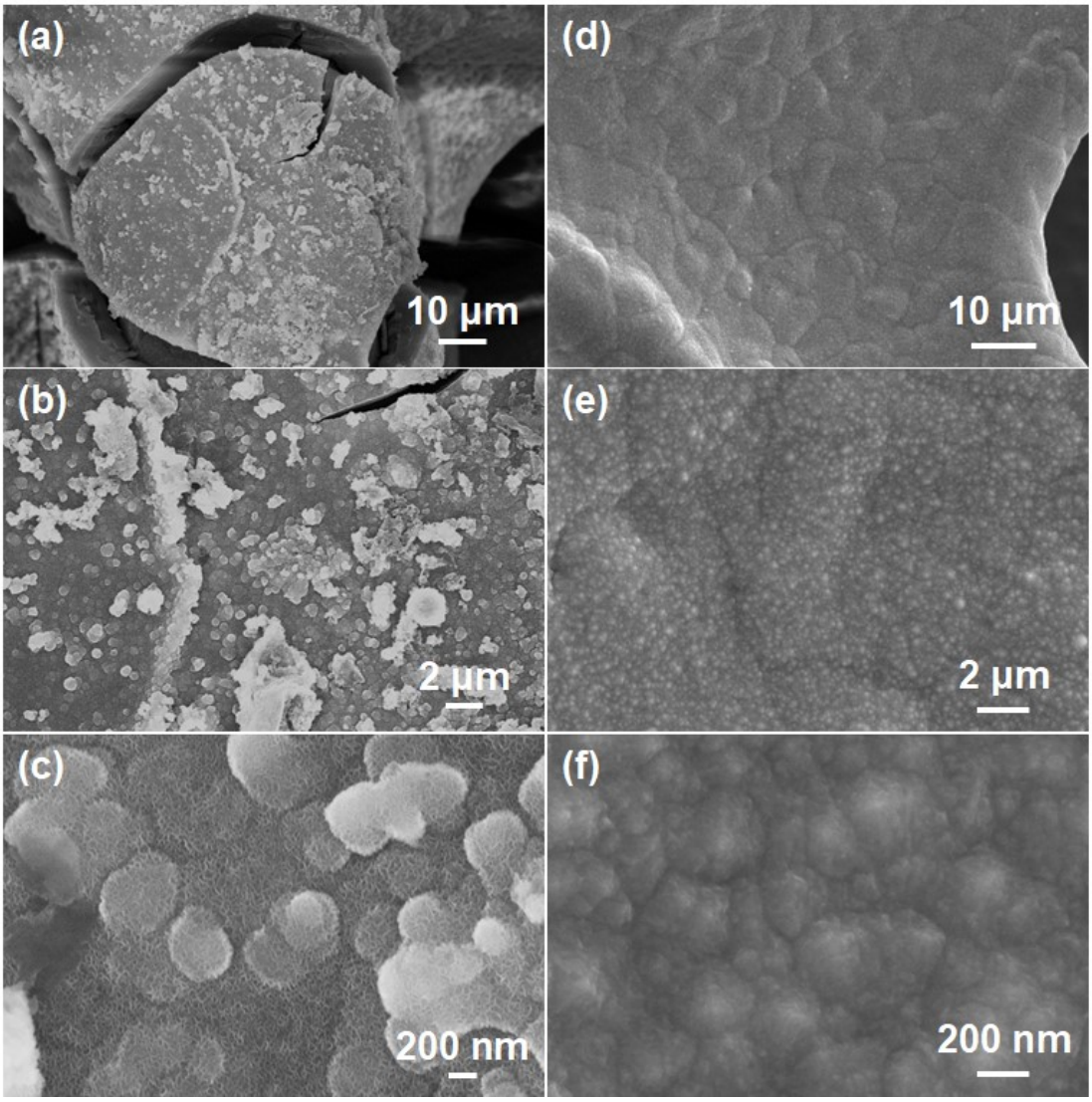

Figure S3. SEM images of (a-c) $Ni(OH)_2$/Ni@Cu and (d-f) Ni@Cu.

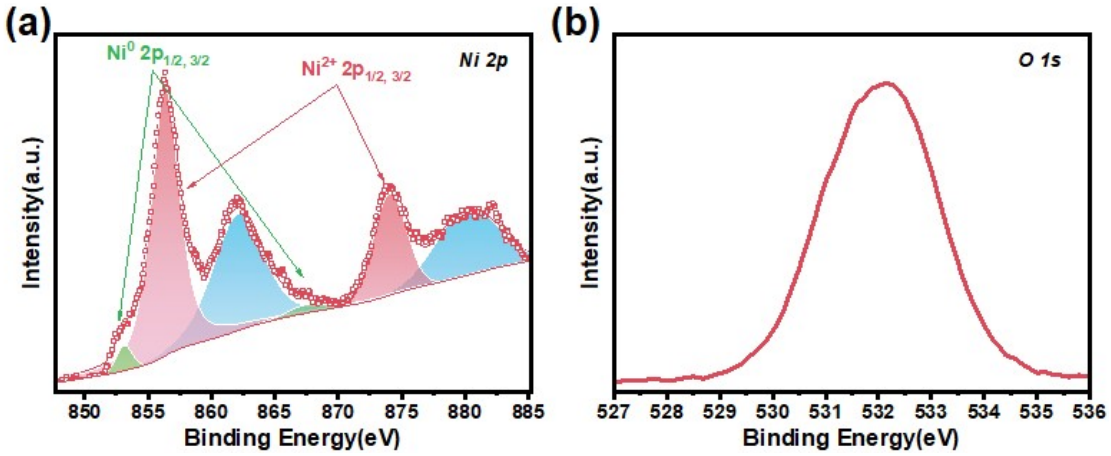

Figure S4. (a) Ni 2p, and (b) O 1s XPS spectra of $Ni(OH)_2$/Ni@Cu.

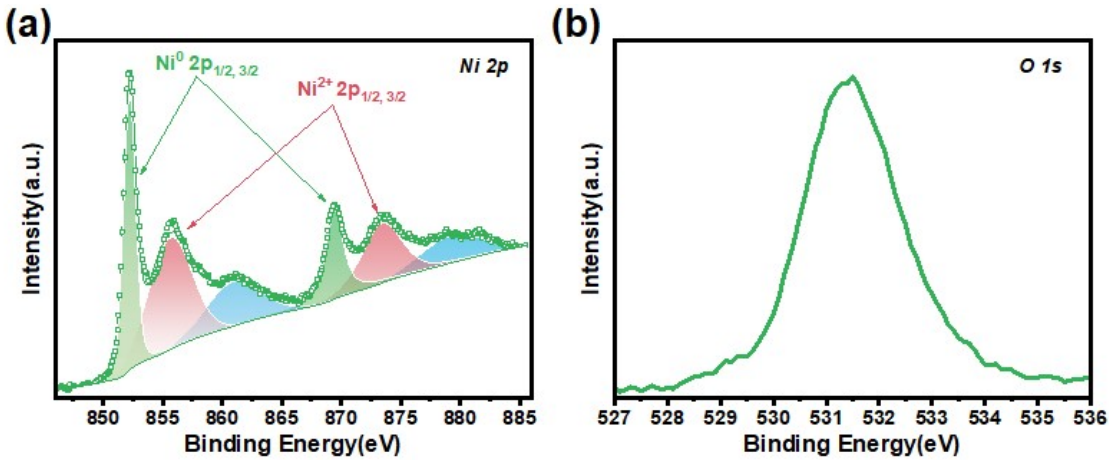

Figure S5. (a) Ni 2p, and (b) O 1s XPS spectra of Ni@Cu.

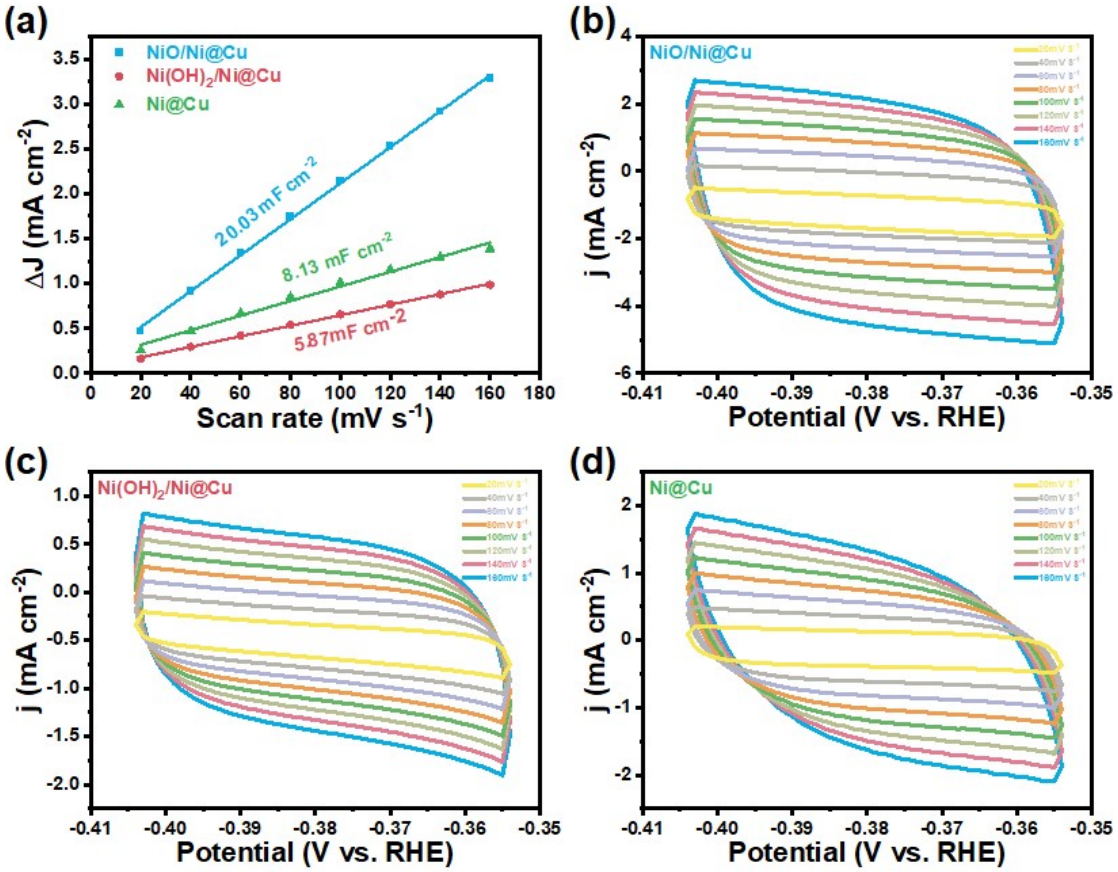

Figure S6. (a) Capacitive current at -0.38V as a function of scan rates (from 20 mV s^{-1} to 160 mV s^{-1}) for NiO/Ni@Cu, $Ni(OH)_2$/Ni@Cu and Ni@Cu. CV curves of (b) NiO/Ni@Cu, (c) $Ni(OH)_2$/Ni@Cu and (d) Ni@Cu at different scan rates.

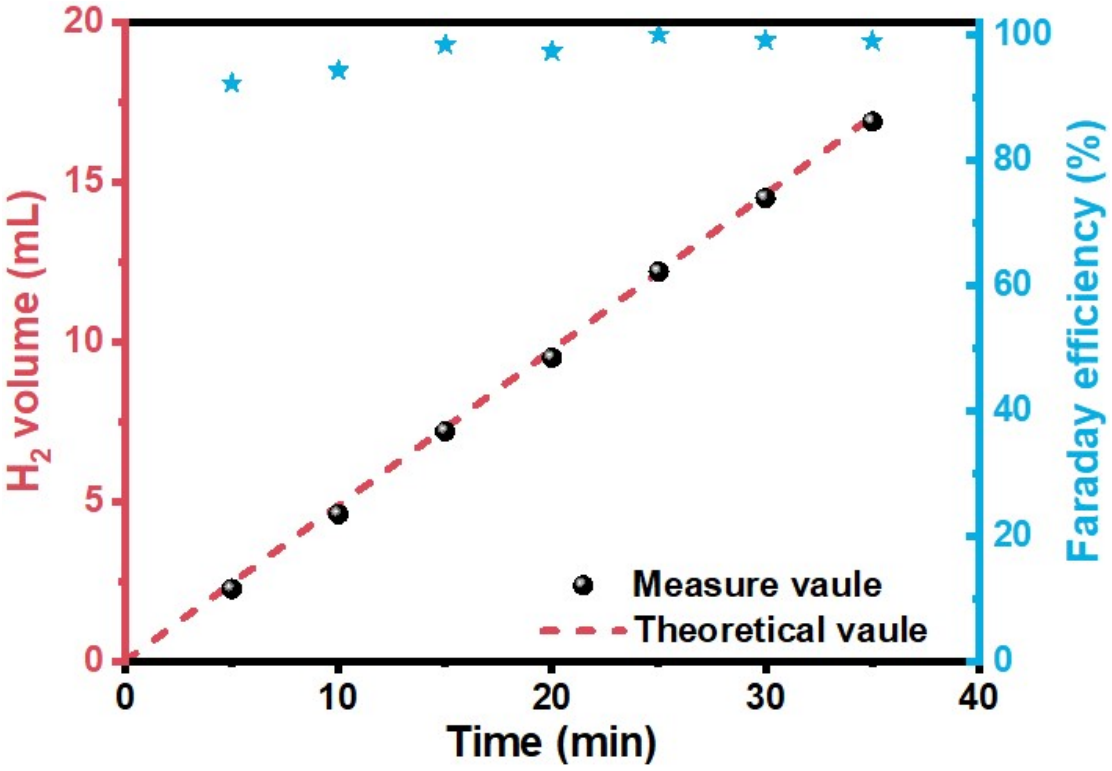

Figure S7. Faraday efficiency of NiO/Ni@Cu in 1 M KOH.

To determine the Faraday efficiency of the HER process, the drainage method was used for measuring the volume of hydrogen produced at a current density of 100 mA cm^{-2}. The Faraday efficiency can be calculated as follows: $\eta = \frac{V \times n \times F}{Q \times V_m}$, where V is the actual hydrogen produced, Q is the total charge passing through the electrolytic cell, V_m is the molar volume of the gas at 298 K, 101 kPa, which has a value of 24.5 L mol^{-1}, F is the Faraday constant, and n is the number of electrons required to produce one

hydrogen molecule. The Faraday efficiency is close to 100% confirming that no side reactions occur during the HER process.

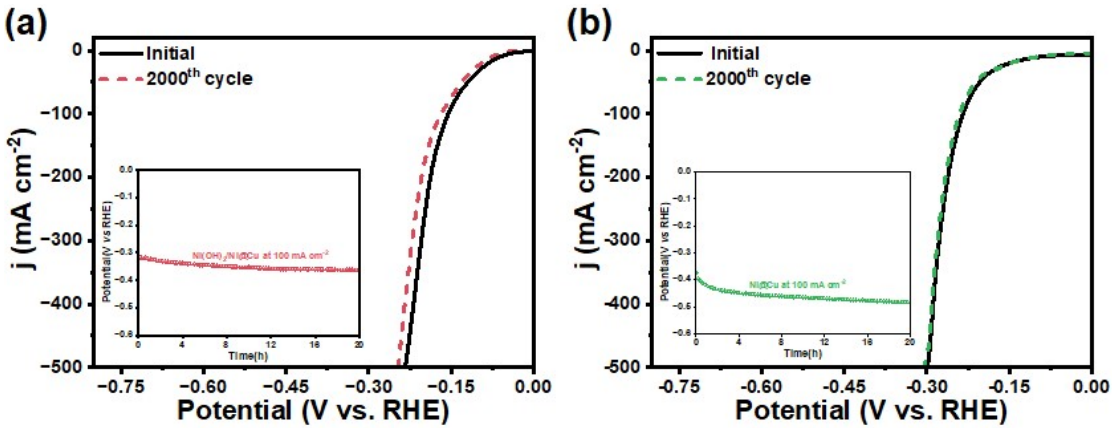

Figure S8. HER polarization curves before and after 2000 cycles of (a) $Ni(OH)_2$/Ni@Cu and (b) Ni@Cu. Inset shows chronopotentiometric response at the density of 100 mA cm^{-2}.

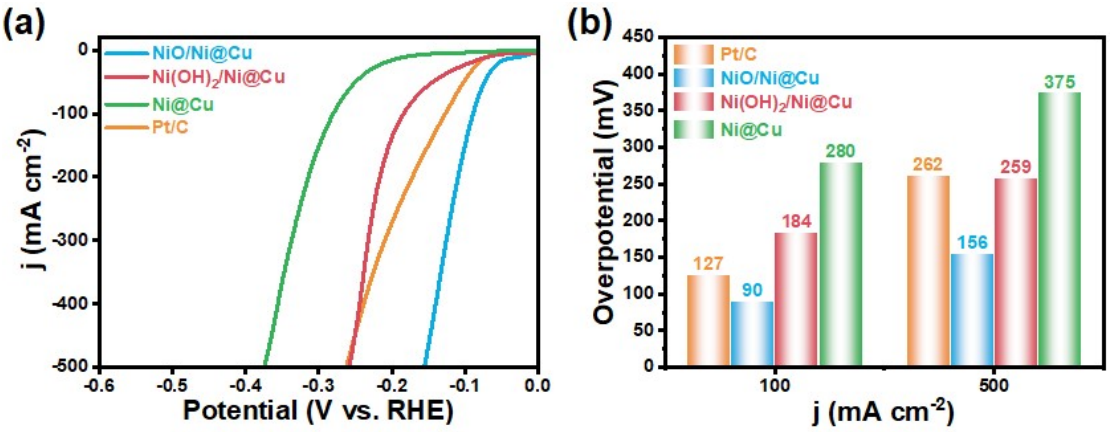

Figure S9. (a) HER polarization curves in 6 M KOH and (b) Comparison of the overpotentials at 100 and 500 mA cm^{-2} with other HER catalysts.

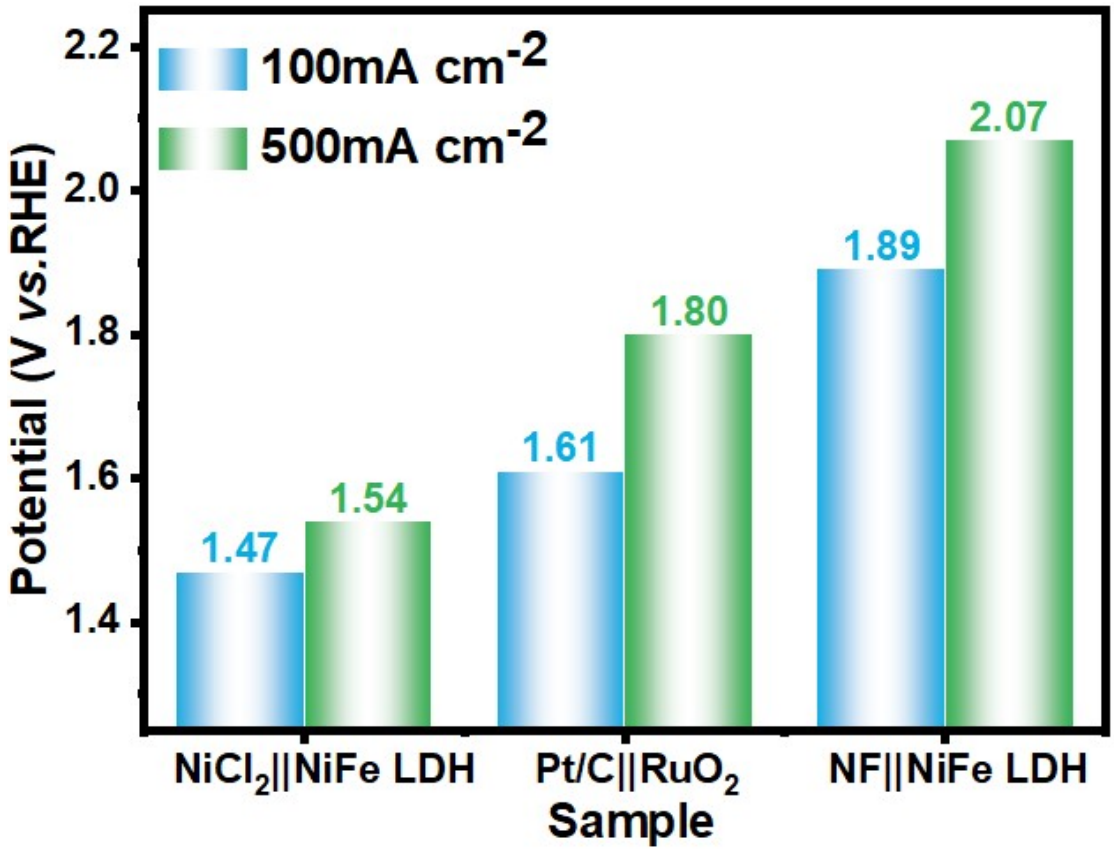

Figure S10. Comparison of the cell voltage at 100 and 500 mA cm^{-2}.

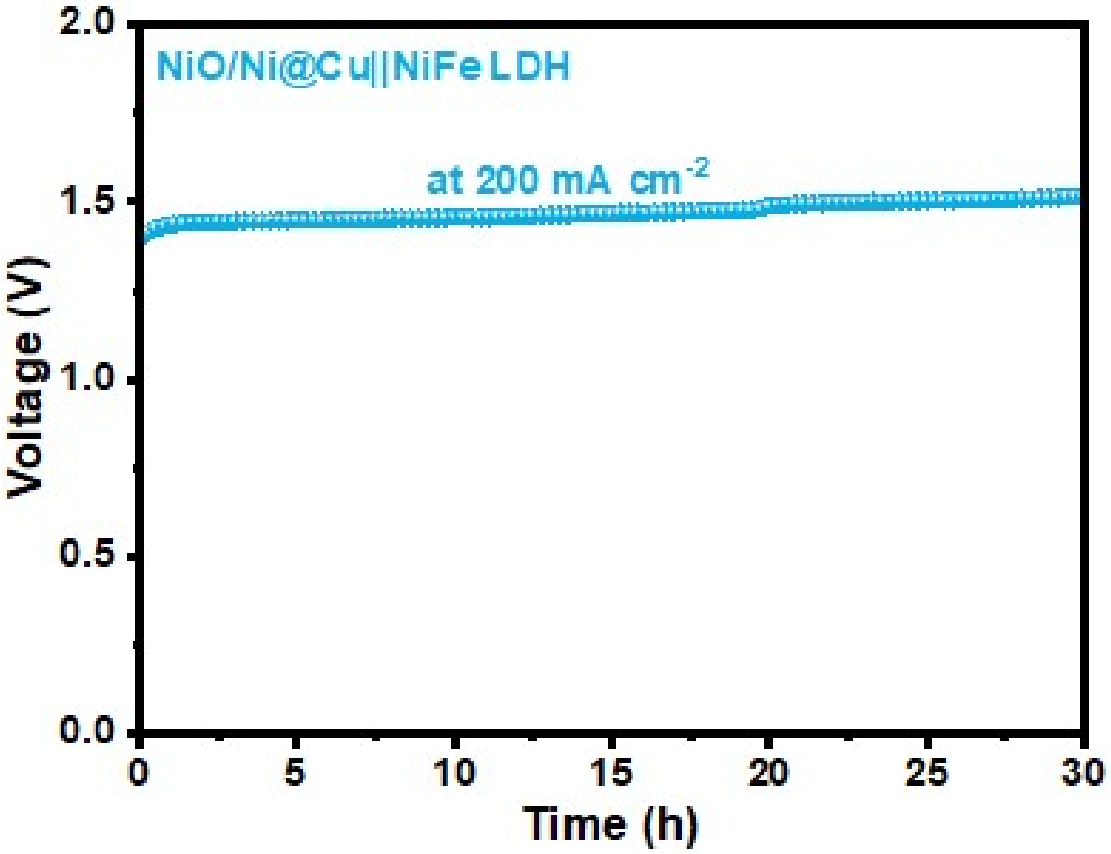

Fig. S11. Chronopotentiometry curve of NiO/Ni@Cu.

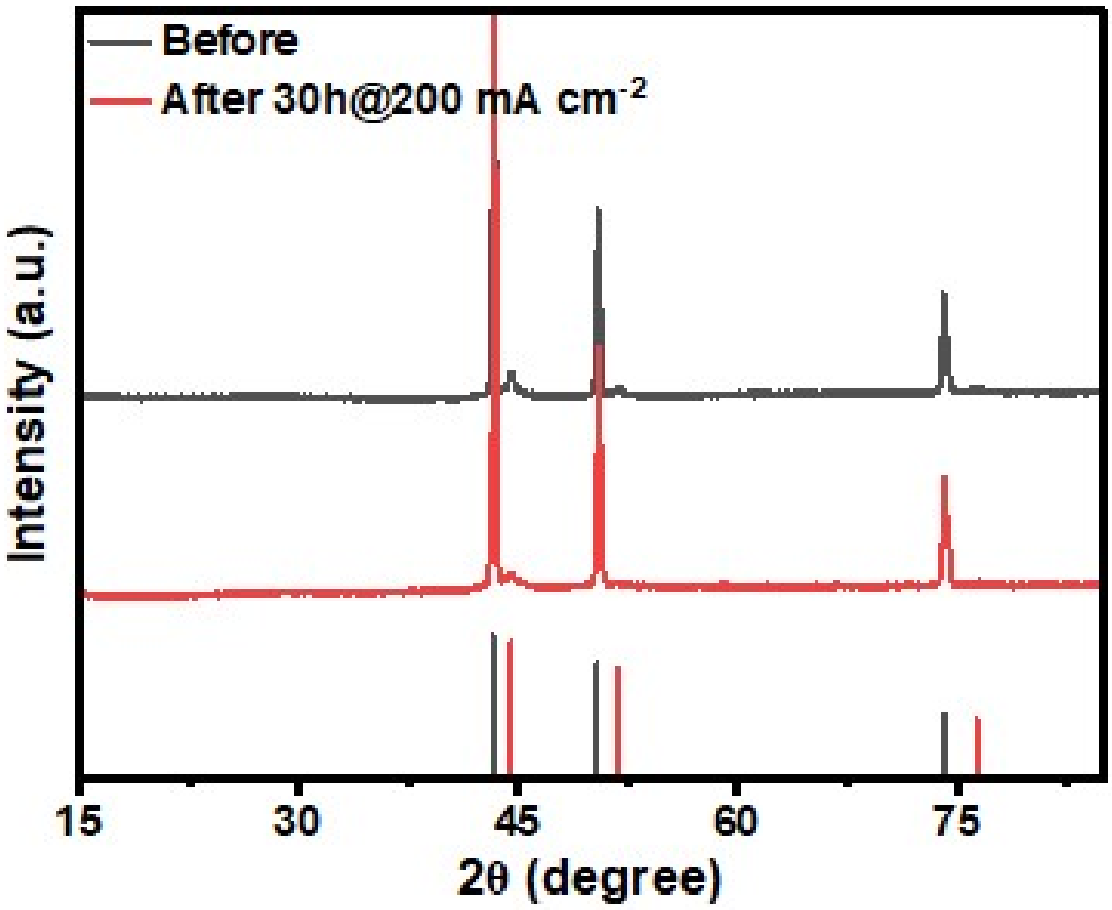

Fig. S12. XRD pattern of NiO/Ni@Cu after stability test.

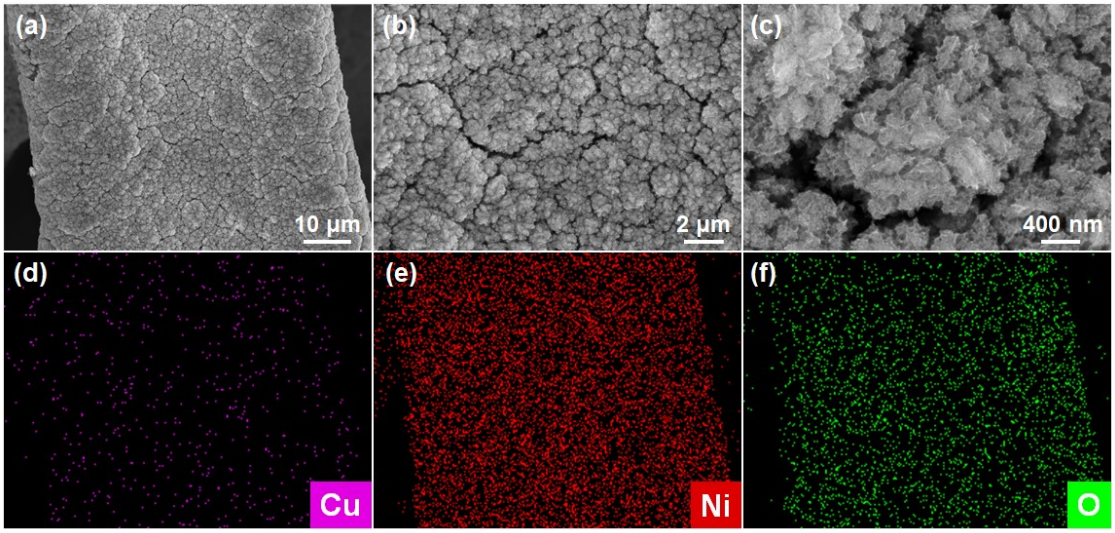

Fig. S13. SEM images and mapping of NiO/Ni@Cu after stability test.

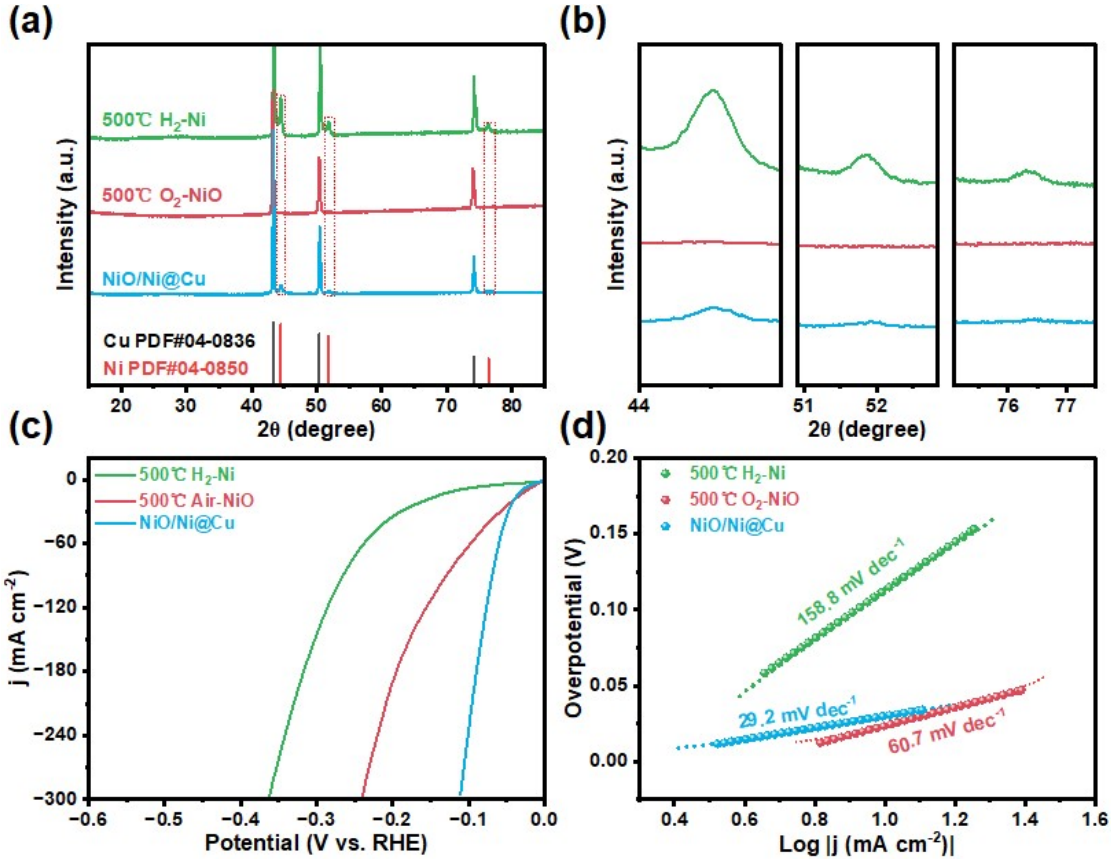

Fig. S14. (a) XRD patterns, (b) Localized enlargement of the corresponding position, (c) HER polarization curves and (d) Tafel slopes of NiO/Ni@Cu, 500 Air-NiO and 500 H_2-Ni.

In order to verify the role of nickel oxide and nickel in alkaline HER, NiO/Ni@Cu were oxidized or reduced in a tube furnace (air or hydrogen argon atmosphere, 500°C for 10 min), and labeled 500 Air-NiO and 500 H_2-Ni, respectively. As showed in Fig. S14a, the XRD patterns show that the peaks attributed to metallic nickel are weakened and strengthened, respectively. The localized zoomed-in view of Fig. S14b highlights this change even more. Although the presence of NiO was not observed in the XRD

pattern of 500 Air-NiO, a change in the composition of NiO/Ni was hypothesized based on the change in the strength of the metal singlet peaks. Specifically, the change is that 500 H_2-Ni contains more nickel metal and 500 Air-NiO contains more NiO.

As shown in the Fig. S14d, NiO/Ni@Cu and 500 Air-NiO exhibit onset potentials close to 0 and lower tafel slopes (29.2, 60.7 mv dec^{-1}, respectively) compared to 500 H_2-Ni with a larger tafel slope (158.8 mv dec^{-1}). According to the classical theory of alkaline electrolyzed water, it is clear that the Tafel and Heyrovsky steps for the determination of NiO/Ni and NiO, respectively. This means that both are not hindered by the volmer reaction ($H_2O + e \rightarrow H_{ads} + OH^-$). Previous calculations have shown that metallic nickel has an appropriate adsorption capacity close to that of platinum (*Nat. Mater.* **2006**, *5* (11), 909–913. *Energy Environ. Sci.* **2013**, *6* (5), 1509). However, due to the lack of metallic nickel as hydrogen adsorption sites on the surface of pure 500 Air-NiO, the HER catalytic activity of NiO/Ni is significantly higher than that of NiO. Therefore, NiO/Ni@Cu combines the water splitting capacity of NiO and the hydrogen adsorption capacity of Ni, showing excellent HER catalytic activity.

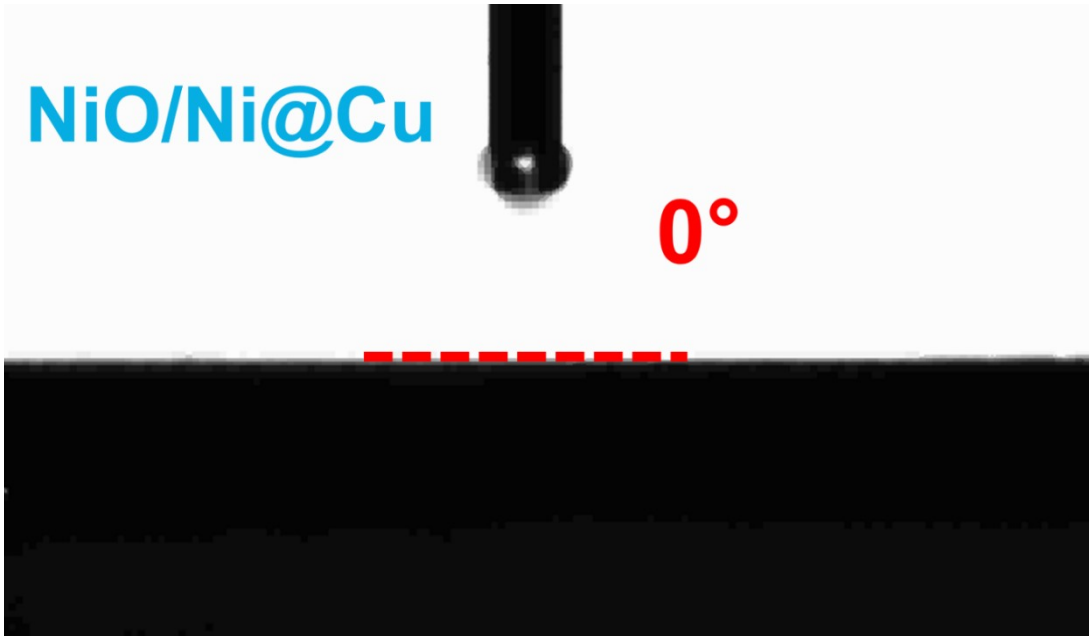

Figure S15. Contact angle measurement of NiO/Ni@Cu.

Table S1. Loading mass of NiO/Ni@Cu, $Ni(OH)_2$/Ni@Cu and Ni@Cu.

Sample	1st (mg)	2nd (mg)	3rd (mg)	Average Laod (mg)
NiO/Ni@Cu	7.68	7.31	7.3	7.43
$Ni(OH)_2$/Ni@Cu	23.74	23.73	24.12	23.86
Ni@Cu	19.85	16.23	15.94	17.34

To determine the catalyst loading, the mass of the electrode sheet was weighed before and after electrodeposition. As shown in Table R1 below, in order to ensure the correctness of the data, three measurements were collected and averaged to obtain the final loading. Sodium dodecyl sulfate facilitates the increase of the precipitation potential of the metal during electrodeposition for rapid nucleation and thus exhibits higher loading at the same electrodeposition voltage. Sodium citrate may promote the formation of the deposit and may enhance the adhesion between the deposit and the substrate, which may enhance the loading of the metal ion nickel onto the substrate. As a result, both $Ni(OH)_2$/Ni and Ni exhibited higher loadings relative to NiO/Ni, which laterally validated the high HER activity of NiO/Ni.

Table S2. Comparison of HER performances for NiO/Ni@Cu with the reported HER catalysts in alkaline eletrolytes.

Electrocatalysts	Substrate	η_{100} (mV)	Stability	iR
NiO/Ni@Cu	CF	60	20h@100mA	95%
TiS_{2-x}/NiS[1]	NF	179	100h@10-100mA cm^{-2}	100%
Ir-Ni/NiO@CNT[2]	GCE	~200	100h@10mA cm^{-2}	95%
MoO_2/Ni@NF[3]	NF	~175	30h@10mA cm^{-2}	100%
M_xO@M_xP/PNCF[4]	NiCo foam	~130	100h@10mA cm^{-2}	90%
Ni/TiO_2 NPAs[5]	CC	~380	17h@~13mA cm^{-2}	98%
Ni_3S_2-MoS_2[6]	NF	~210	24h@10mA cm^{-2}	75%
Ru@Ni-MOF[7]	NF	~105	24h@10mA cm^{-2}	100%
N-NiMoS[8]	NF	~150	1000h@~20mA cm^{-2}	90%
TMP NiZn-Ni/NF[9]	NF	115	100h@~40mA cm^{-2}	90%
Ni-Mo_2C-0.67[10]	Ni plate	194	100h@~15 mA cm^{-2}	100%
Ni-MoO_2[11]	GCE	~356	24h@10 mA cm^{-2}	100%
Ni-Mo_2C@NPC[12]	GCE	~260	12h@~20 mA cm^{-2}	Without

Table S3. Comparison of the voltages required to achieve a current density of 100 mA cm^{-2} for overall water splitting between the NiO/Ni@Cu||NiFe LDH pair and other transition metal-based catalysts in alkaline eletrolytes.

Electrocatalysts	Substrate	$Voltage_{100}$ (V)	Stability	iR
NiO/Ni@Cu||NiFe LDH	CF	1.47	200h@100mA^{-2}	95%
CuNi@NiFeCu[13]	CP	~1.8	50h@~90mA cm^{-2}	90%
LSC/K-$MoSe_2$[14]	NF	1.95	2500h@100mA cm^{-2}	100%
NiCoP-WO_x||NiFeP-WO_x[15]	NF	~1.72	16h@10mA cm^{-2}	100%
NiP_2/$NiSe_2$[16]	CF	1.8	30h@10mA cm^{-2}	95%
Ni_2P-Fe_2P/NF[17]	NF	1.68	48h@100mA cm^{-2}	100%
Co_8FeV[18]	CC	1.65	100h@100mA cm^{-2}	95%
Mo-NiP_x/NiS_y[19]	NF	1.7	27h@10mA cm^{-2}	95%
MoO_3/Ni–NiO[20]	CC	~1.8	20h@10mA cm^{-2}	100%
NIS-450[21]	Ni foil	1.69	10h@10mA cm^{-2}	Without
Ni–Fe–Mn–P/NC[22]	NF	~1.62	35h@10mA cm^{-2}	100%
Ni-MoN||SSM[23]	CF	1.61	~100h@100mA cm^{-2}	100%
Ni-Co-Fe-P NBs[24]	NF	~1.55	100h@100mA cm^{-2}	100%
Ni/Mo-Ni[25]	NF	1.76	87h@100mA cm^{-2}	100%
$MoNi_4$/MoO_2||FeCoNiS[26]	NF	1.6	1200h@200mA cm^{-2}	Without

RuFe@NF[27]	NF	~1.82	680h@100mA cm^{-2}	100%
NiFeCoSx@$FeNi_3$[28]	FeNi3 foam	~1.8	80h@10mA cm^{-2}	Without
N-MoS_2·Ni_3S_2/NiS[29]	NF	~1.9	30h@10mA cm^{-2}	100%
Ni_3S_2/Cu–NiCo LDH/NF[30]	NF	1.75	12h@100mA cm^{-2}	90%
Ni-MoC@NCNT/CC-2[31]	CC	1.68	30h@~100mA cm^{-2}	100%
$NiSe_2$/Ni_3Se_4/NF[32]	NF	~1.72	36h@10mA cm-2	80%

Reference

1. J. Wu, W. Zhong, C. Yang, W. Xu, R. Zhao, H. Xiang, Q. Zhang, X. Li and N. Yang, *Appl. Catal., B: Environ.*, 2022, **310**, 121332.
2. J. Liu, Z. Wang, D. Zhang, Y. Qin, J. Xiong, J. Lai and L. Wang, *Small*, 2022, **18**, 2108072.
3. W. Liang, P. Dong, Z. Le, X. Lin, X. Gong, F. Xie, H. Zhang, J. Chen, N. Wang, Y. Jin and H. Meng, *ACS Appl. Mater. Inter.*, 2021, **13**, 39470-39479.
4. Q. Zhang, W. Chen, G. Chen, J. Huang, B. Ouyang, D. Chen, E. Kan, T. Lan, C. Li, H.-S. Choi and K. K. Ostrikov, *ACS Sustain. Chem. Eng.*, 2021, **9**, 7454-7465.
5. Y. Li, K.-A. Min, B. Han and L. Y. S. Lee, *Appl. Catal., B: Environ.*, 2021, **282**, 119548.
6. S. Yang, Y. Guo, Y. Zhao, L. Zhang, H. Shen, J. Wang, J. Li, C. Wu, W. Wang, Y. Cao, S. Zhuo, Q. Zhang and H. Zhang, *Small*, 2022, **18**, 2201306.
7. L. Deng, F. Hu, M. Ma, S.-C. Huang, Y. Xiong, H.-Y. Chen, L. Li and S. Peng, *Angew. Chem., Int. Ed.*, 2021, **60**, 22276-22282.
8. C. Huang, L. Yu, W. Zhang, Q. Xiao, J. Zhou, Y. Zhang, P. An, J. Zhang and Y. Yu, *Appl. Catal., B: Environ.*, 2020, **276**, 119137.
9. Q. Zhou, Q. Hao, Y. Li, J. Yu, C. Xu, H. Liu and S. Yan, *Nano Energy*, 2021, **89**, 106402.
10. W. Liu, X. Wang, J. Qu, X. Liu, Z. Zhang, Y. Guo, H. Yin and D. Wang, *Appl. Catal., B: Environ.*, 2022, **307**, 121201.
11. T. Yang, Y. Xu, H. Lv, M. Wang, X. Cui, G. Liu and L. Jiang, *ACS Sustain. Chem. Eng.*, 2021, **9**, 13106-13113.
12. Y. Lu, C. Yue, Y. Li, W. Bao, X. Guo, W. Yang, Z. Liu, P. Jiang, W. Yan, S. Liu, Y. Pan and Y. Liu, *Appl. Catal., B: Environ.*, 2021, **296**, 120336.
13. D. Cao, H. Xu and D. Cheng, *Appl. Catal., B: Environ.*, 2021, **298**, 120600.
14. N. K. Oh, J. Seo, S. Lee, H.-J. Kim, U. Kim, J. Lee, Y.-K. Han and H. Park, *Nat. Commun.*, 2021, **12**, 4606.
15. D. Kim, Y. Jeong, H. Roh, C. Lim and K. Yong, *J. Mater. Chem. A*, 2021, **9**, 10909-10920.
16. L. Yang, L. Huang, Y. Yao and L. Jiao, *Appl. Catal., B: Environ.*, 2021, **282**, 119584.
17. L. Wu, L. Yu, F. Zhang, B. McElhenny, D. Luo, A. Karim, S. Chen and Z. Ren, *Adv. Funct. Mater.*, 2021, **31**, 2006484.
18. J. Lv, P. Liu, R. Li, L. Wang, K. Zhang, P. Zhou, X. Huang and G. Wang, *Appl. Catal., B: Environ.*, 2021, **298**, 120587.

19. J. Wang, M. Zhang, G. Yang, W. Song, W. Zhong, X. Wang, M. Wang, T. Sun and Y. Tang, *Adv. Funct. Mater.*, 2021, **31**, 2101532.

20. X. Li, Y. Wang, J. Wang, Y. Da, J. Zhang, L. Li, C. Zhong, Y. Deng, X. Han and W. Hu, *Adv. Mater.*, 2020, **32**, 2003414.

21. G. Bahuguna, A. Cohen, N. Harpak, B. Filanovsky and F. Patolsky, *Small Methods*, 2022, **6**, 2200181.

22. R. B. Ghising, U. N. Pan, D. R. Paudel, M. R. Kandel, N. H. Kim and J. H. Lee, *J. Mater. Chem. A*, 2022, **10**, 16457-16467.

23. L. Wu, F. Zhang, S. Song, M. Ning, Q. Zhu, J. Zhou, G. Gao, Z. Chen, Q. Zhou, X. Xing, T. Tong, Y. Yao, J. Bao, L. Yu, S. Chen and Z. Ren, *Adv. Mater.*, 2022, **34**, 2201774.

24. A. Li, L. Zhang, F. Wang, L. Zhang, L. Li, H. Chen and Z. Wei, *Appl. Catal., B: Environ.*, 2022, **310**, 121353.

25. H. Li, C. Cai, Q. Wang, S. Chen, J. Fu, B. Liu, Q. Hu, K. Hu, H. Li, J. Hu, Q. Liu, S. Chen and M. Liu, *Chem. Eng. J.*, 2022, **435**, 134860.

26. Y. Huang, L.-W. Jiang, H. Liu and J.-J. Wang, *Chem. Eng. J.*, 2022, **441**, 136121.

27. H. Liu, Q. Jia, S. Huang, L. Yang, S. Wang, L. Zheng and D. Cao, *J. Mater. Chem. A*, 2022, **10**, 4817-4824.

28. J. Shen, Q. Li, W. Zhang, Z. Cai, L. Cui, X. Liu and J. Liu, *J. Mater. Chem. A*, 2022, **10**, 5442-5451.

29. Y. Gao, J. Li, H. Gong, C. Zhang, H. Fan, X. Xie, X. Huang, H. Xue, T. Wang and J. He, *J. Mater. Chem. A*, 2022, **10**, 11755-11765.

30. L. Jia, G. Du, D. Han, Y. Hao, W. Zhao, Y. Fan, Q. Su, S. Ding and B. Xu, *J. Mater. Chem. A*, 2021, **9**, 27639-27650.

31. B. Geng, F. Yan, L. Liu, C. Zhu, B. Li and Y. Chen, *Chem. Eng. J.*, 2021, **406**, 126815.

32. L. Tan, J. Yu, H. Wang, H. Gao, X. Liu, L. Wang, X. She and T. Zhan, *Appl. Catal., B: Environ.*, 2022, **303**, 120915.